

Signal estimation bias in x-ray dark-field imaging using dual phase grating interferometer

Zhi-Li Wang(王志立), Zun Zhang(张尊), Heng Chen(陈恒), and Xin Ge(葛昕)

Citation: Chin. Phys. B, 2025, 34 (**3**): 038701. DOI: 10.1088/1674-1056/ada430
Journal homepage: http://cpb.iphy.ac.cn; http://iopscience.iop.org/cpb

What follows is a list of articles you may be interested in

Investigations of moiré artifacts induced by flux fluctuations in x-ray dark-field imaging

Zhi-Li Wang(王志立), Zi-Han Chen(陈子涵), Yao Gu(顾瑶), Heng Chen(陈恒), and Xin Ge(葛昕)
Chin. Phys. B, 2023, 32 (**3**): 038704. DOI: 10.1088/1674-1056/ac946a

Analysis of refraction and scattering image artefacts in x-ray analyzer-based imaging

Li-Ming Zhao(赵立明), Tian-Xiang Wang(王天祥), Run-Kang Ma(马润康), Yao Gu(顾瑶), Meng-Si Luo(罗梦丝), Heng Chen(陈恒), Zhi-Li Wang(王志立), and Xin Ge(葛昕)
Chin. Phys. B, 2023, 32 (**2**): 028701. DOI: 10.1088/1674-1056/ac685d

Quantitative coherence analysis of dual phase grating x-ray interferometry with source grating

Zhi-Li Wang(王志立), Rui-Cheng Zhou(周瑞成), Li-Ming Zhao(赵立明), Kun Ren(任坤), Wen Xu(徐文), Bo Liu(刘波), and Heng Chen(陈恒)
Chin. Phys. B, 2021, 30 (**2**): 028702. DOI: 10.1088/1674-1056/abb7fd

Retrieval of multiple scattering contrast from x-ray analyzer-based imaging

Heng Chen(陈恒), Bo Liu(刘波), Li-Ming Zhao(赵立明), Kun Ren(任坤), and Zhi-Li Wang(王志立)
Chin. Phys. B, 2021, 30 (**1**): 018701. DOI: 10.1088/1674-1056/abbbed

Biases of estimated signals in x-ray analyzer-based imaging

Jianlin Xia(夏健霖), Wen Xu(徐文), Ruicheng Zhou(周瑞成), Xiaomin Shi(石晓敏), Kun Ren(任坤), Heng Chen(陈恒), Zhili Wang(王志立)
Chin. Phys. B, 2020, 29 (**6**): 068703. DOI: 10.1088/1674-1056/ab8887

Signal estimation bias in x-ray dark-field imaging using dual phase grating interferometer

Zhi-Li Wang(王志立)[1,†], Zun Zhang(张尊)[1], Heng Chen(陈恒)[1], and Xin Ge(葛昕)[2]

[1] *School of Physics, Hefei University of Technology, Hefei* 230009, *China*
[2] *School of Science, Shenzhen Campus of Sun Yat-sen University, Shenzhen* 518107, *China*

(Received 10 October 2024; revised manuscript received 5 December 2024; accepted manuscript online 31 December 2024)

In x-ray dark-field imaging using dual phase grating interferometer, multi-contrast signals are extracted from a set of acquired phase-stepping data by using the least-squares fitting algorithm. The extracted mean intensity, amplitude and visibility signals may be intrinsically biased. However, it is still unclear how large these biases are and how the data acquisition parameters influence the biases in the extracted signals. This work set out to address these questions. Analytical expressions of the biases of the extracted signals were theoretically derived by using a second-order Taylor series expansion. Extensive numerical simulations were performed to validate the theoretical results. It is illustrated that while the estimated mean intensity signal is always unbiased, the estimated amplitude and visibility signals are both positively biased. While the biases of the estimated amplitude signals are proportional to the inverse of the total number of phase steps, the biases of the estimated visibility signals are inversely proportional to the product of the total number of phase steps and the mean number of photons counted per phase step. Meanwhile, it is demonstrated that the dependence of the biases on the mean visibility is quite different from that of Talbot–Lau interferometer due to the difference in the intensity model. We expect that these results can be useful for data acquisition optimizations and interpretation of x-ray dark-field images.

Keywords: x-ray imaging, dual phase grating interferometer, dark-field imaging, signal bias

PACS: 87.59.–e, 87.64.mf, 07.60.Ly, 43.60.Cg

DOI: 10.1088/1674-1056/ada430 **CSTR:** 32038.14.CPB.ada430

1. Introduction

In recent years, x-ray dual phase grating interferometry has demonstrated its attractive advantages as a multi-contrast imaging technique.[1–16] Different from Talbot–Lau interferometry,[17–24] dual phase grating interferometry utilizes two fine-pitch phase gratings to generate moiré fringes with a pitch hundreds of times greater than that of phase gratings. As a consequence, dual phase grating interferometry enables efficient use of common imaging detectors to resolve the moiré fringes directly. Furthermore, working with pure phase gratings enables radiation dose reduction by a factor of approximately two, and resolves the challenge of fabricating absorbing gratings of high aspect ratio and large area.[1,2] Most importantly, dual phase grating interferometry allows tunable dark-field sensitivity by varying the inter-grating distance.[2,16] Kagias *et al*. demonstrated the advantage of tunable dark-field sensitivity by imaging powders of different mean grain sizes.[2] From dark-field images at different correlation lengths, significant change in the dark-field signal strength for the two different powders can be clearly seen. Therefore, tunable dark-field imaging provides a more straightforward way to reveal the relation between the correlation length and the sample's dark-field signal. This relation is the key to quantitatively accessing the sub-micron structural information of the sample.[25,26] Quite recently, Organista *et al*. demonstrated the implementation of x-ray dual phase grating interferometer for building materials characterization in a nanoscale range, with samples of tens of millimeters in size, validated with dark-field images at different correlation lengths.[16]

Dual-phase grating interferometer can be operated in two imaging modes. In the single shot mode, the image resolution is defined by the pitch of moiré fringes, which varies significantly between measurements at different correlation lengths.[3] Consequently, image registration becomes mandatory for further analysis, which is unfavorable for tunable dark-field imaging. By contrast, in the phase-stepping mode the resolution of the imaging detector is maintained, which enables tunable dark-field sensitivity without image registration. Therefore, the phase-stepping approach is commonly used for intensity data acquisition.[2,7,9,11,13–16] In a phase-stepping procedure, one of the gratings is laterally shifted over one or more periods in a total of M phase steps, and an intensity measurement is performed by the detector at each grating position.

According to theoretical models of x-ray dual phase grating interferometry, in the absence of noise, a phase-stepping acquisition leads to the following intensity profile for each detector pixel:[8,12]

$$\bar{N}_k(x,y) = \bar{N}_0 + \bar{N}_1 \cos\left(\bar{\phi} + \frac{2\pi k}{M}\right)$$

†Corresponding author. E-mail: dywangzl@hfut.edu.cn

© 2025 Chinese Physical Society and IOP Publishing Ltd. All rights, including for text and data mining, AI training, and similar technologies, are reserved.

$$+\bar{N}_2\cos\left(2\bar{\phi}+\frac{4\pi k}{M}\right),\quad (k=1,2,\ldots,M), \tag{1}$$

where (x,y) denotes the pixel coordinates in a two-dimensional detector array, $\bar{N}_k$ is the expected x-ray intensity measured at the k^{th} phase step, and the total number of phase steps M satisfies $M \geq 5$ for multi-contrast signal retrieval. The mean intensity N_0 (i.e., the mean number of photons counted per phase step) is related to the absorption contrast signal, and the phase coefficient ϕ to the differential phase contrast signal. As experimentally validated,[12,16] both the first-order and second-order harmonics contribute to the measured intensity, represented by the amplitudes N_1 and N_2 in Eq. (1), respectively. Especially, when using polychromatic sources, the first-order harmonic always dominates the contribution to the fringe intensity for dual $\pi/2$-grating setups, while the second-order harmonic dominates the fringe intensity for dual π-grating setups.[8,11] The amplitudes are directly related to the 1st and 2nd visibilities by $V_1 = N_1/N_0$ and $V_2 = N_2/N_0$, respectively. Especially, when performing tunable dark-field imaging, it is the visibility V_1 or V_2 that determines the noise behavior of the retrieved dark-field images, rather than the overall fringe visibility. Finally, the dark-field signal can be accessed from a relative visibility reduction resulting from small-angle scattering within the investigated sample.[25,26]

As x-ray dual phase grating interferometers work with photon-limited polychromatic tube sources, each x-ray intensity measurement is inevitably contaminated by noise. In order to accurately extract different contrast signals, intensity measurements should be repeated many times and averaged at each phase step. One can estimate the expected photon number at each phase step (i.e., $\bar{N}_k$), which is then used to extract multi-contrast signals. However, due to the concerns of potential risks associated with ionizing radiation, repeated intensity measurements are impractical in clinically medical imaging. Therefore, one question encountered in multi-contrast signal retrieval process is, how does one seek for a set of four characteristic parameters, $\{N_0, N_1, N_2, \phi\}$, that best fits a single set of measured phase-stepping data N_k? As a natural choice to address this question, a least-squares fitting algorithm can be utilized to accomplish this goal.[27] A closed-form solution for $\{N_0, N_1, N_2, \phi\}$, denoted as $\{\hat{N}_0, \hat{N}_1, \hat{N}_2, \hat{\phi}\}$, can be derived from a least-squares optimization problem, as shown below.

However, one fundamental question that remains to be addressed is how accurate are the parameters extracted by using a least-squares fitting algorithm? In Talbot–Lau interferometry, Ji *et al*. presented theoretical and experimental studies of estimation biases of the absorption, differential phase, and dark-field contrast signals extracted by a least-squares fitting algorithm.[28] It was shown that while the estimated absorption signal is unbiased, the estimated dark-field signal is positively biased, with the relative bias dependent on the mean visibility and the exposure level. However, to the best of our knowledge, the potential bias of the extracted multi-contrast signals, as a quantitative measure of the signal estimation accuracy, has not yet been fully addressed in x-ray dual phase grating interferometry. The purpose of this work is to perform both theoretical and numerical studies on this topic in x-ray dark-field imaging using dual phase grating interferometers. Specifically, we aim to address the following intriguing questions: (1) Is the least-squares fitting signal estimation a biased estimator? (2) If biased, how large is the estimation bias? and (3) how do the data acquisition parameters influence the estimation bias? Finally, noting the significant difference in the intensity model, one can reasonably expect that the signal estimation biases are different from those of Talbot–Lau interferometer.[28]

The paper is structured as follows. Section 2 briefly reviews theoretical formulas for multi-contrast signal estimation using the least-squares fitting algorithm, and then presents analytical formulas of signal estimation biases by using a second-order Taylor series expansion. Section 3 presents results of numerical simulations to validate theoretical formulas derived in Section 2. Finally, discussions and conclusion are presented in Section 4. We expect that these results can be useful for interpretation of x-ray dark-field images.

2. Theory and methods

2.1. Multi-contrast signal estimation using least-squares fitting

With a set of measured phase-stepping data N_k $(k=1,2,\ldots,M)$, signal estimation using the least-squares fitting algorithm can be formulated as the following local minimization problem:

$$\begin{aligned}&\{\hat{N}_0,\hat{N}_1,\hat{N}_2,\hat{\phi}\}\\ =&\underset{N_0,N_1,N_2,\phi}{\arg\min}\sum_{k=1}^{M}\left\{N_k-\left[N_0+N_1\cos\left(\phi+2\pi\frac{k}{M}\right)\right.\right.\\&\left.\left.+N_2\cos\left(2\phi+4\pi\frac{k}{M}\right)\right]\right\}^2.\end{aligned} \tag{2}$$

By calculating the partial derivatives of the least-squared objective function with respect to the four parameters N_0, N_1, N_2 and ϕ, one can readily obtain a closed-form solution to the minimization problem given by Eq. (2),

$$\hat{N}_0=\frac{1}{M}\sum_{k=1}^{M}N_k, \tag{3}$$

$$\hat{N}_1=\frac{2}{M}\sqrt{\left[\sum_{k=1}^{M}N_k\sin\left(2\pi\frac{-k}{M}\right)\right]^2+\left[\sum_{k=1}^{M}N_k\cos\left(2\pi\frac{k}{M}\right)\right]^2}, \tag{4}$$

$$\hat{N}_2=\frac{2}{M}\sqrt{\left[\sum_{k=1}^{M}N_k\sin\left(4\pi\frac{-k}{M}\right)\right]^2+\left[\sum_{k=1}^{M}N_k\cos\left(4\pi\frac{k}{M}\right)\right]^2}. \tag{5}$$

As the main benefit of dual phase grating interferometry lies in tunable dark-field imaging without image registration, this work focuses on the potential biases of the estimated mean intensity and amplitude coefficients, and finally the visibility signals. Equations (3)–(5) lead to the following formulas for retrieving visibility signals:

$$\hat{V}_1 = 2\times\sqrt{\left[\sum_{k=1}^{M} N_k \sin\left(2\pi\frac{-k}{M}\right)\right]^2 + \left[\sum_{k=1}^{M} N_k \cos\left(2\pi\frac{k}{M}\right)\right]^2} \Big/ \sum_{k=1}^{M} N_k, \tag{6}$$

$$\hat{V}_2 = 2\times\sqrt{\left[\sum_{k=1}^{M} N_k \sin\left(4\pi\frac{-k}{M}\right)\right]^2 + \left[\sum_{k=1}^{M} N_k \cos\left(4\pi\frac{k}{M}\right)\right]^2} \Big/ \sum_{k=1}^{M} N_k. \tag{7}$$

2.2. Potential estimation bias of an estimator

In statistics, the bias of an estimated parameter $\hat{\theta}$ is defined as the statistical mean of the difference between the estimated value and its truth θ,

$$b_\theta\left(\hat{\theta}\right) = E\left(\hat{\theta}-\theta\right) = \int\left[\hat{\theta}\left(\boldsymbol{x}\right)-\theta\right]P\left(\boldsymbol{x};\theta\right)\mathrm{d}\boldsymbol{x}, \tag{8}$$

where $\boldsymbol{x}$ denotes the measured data vector from which the estimator $\hat{\theta}$ is extracted, and $P(\boldsymbol{x};\theta)$ is the probability density function of $\boldsymbol{x}$ for a given θ. In practice, it may be difficult or even impossible to directly and analytically calculate the integration in Eq. (8). Alternatively, one can proceed by using a Taylor series expansion around $\bar{x}$ to approximate $\hat{\theta}$ as follows:[28,29]

$$\begin{aligned}\hat{\theta}\left(\boldsymbol{x}\right) \cong\ & \hat{\theta}\left(\bar{\boldsymbol{x}}\right) + \sum_i \left.\frac{\partial\hat{\theta}}{\partial x_i}\right|_{\bar{\boldsymbol{x}}}\left(x_i-\bar{x}_i\right) + \frac{1}{2}\sum_{i,j}\left.\frac{\partial^2\hat{\theta}}{\partial x_i\partial x_j}\right|_{\bar{\boldsymbol{x}}} \\ & \times\left(x_i-\bar{x}_i\right)\left(x_j-\bar{x}_j\right),\end{aligned} \tag{9}$$

where x_i denotes the i^{th} element in the data vector. Under this approximation, one can obtain the statistical mean of the estimated parameter as

$$\begin{aligned}E\left[\hat{\theta}\left(\boldsymbol{x}\right)\right] \cong\ & \hat{\theta}\left(\bar{\boldsymbol{x}}\right) + \sum_i \left.\frac{\partial\hat{\theta}}{\partial x_i}\right|_{\bar{\boldsymbol{x}}}\left\langle x_i-\bar{x}_i\right\rangle + \frac{1}{2}\sum_{i,j}\left.\frac{\partial^2\hat{\theta}}{\partial x_i\partial x_j}\right|_{\bar{\boldsymbol{x}}} \\ & \times\left\langle\left(x_i-\bar{x}_i\right)\left(x_j-\bar{x}_j\right)\right\rangle,\end{aligned} \tag{10}$$

where $\langle\cdot\rangle$ denotes ensemble averaging. As dual phase grating interferometers using polychromatic x-ray tubes are always photon limited, the measured phase-stepping data can be considered as uncorrelated and Poisson distributed random variables. Then the bias of an estimator $\hat{\theta}$ can be approximately calculated by using Eqs. (8) and (10). And the final result is given by

$$b_\theta\left(\hat{\theta}\right) = \left\langle\hat{\theta}\right\rangle - \bar{\theta} \cong \frac{1}{2}\sum_i \left.\frac{\partial^2\hat{\theta}}{\partial x_i^2}\right|_{\bar{\boldsymbol{x}}}\sigma_{x_i}^2. \tag{11}$$

That is, the bias of θ is determined by the second-order derivative of the estimator calculated based on the expected value of $\bar{\boldsymbol{x}}$ and the variance of the measured data.

2.3. Bias of mean intensity estimator

By use of the closed-form solution of $\hat{N}_0$ given by Eq. (3), the second-order derivative of $\hat{N}_0$ with respect to N_k can be readily calculated as

$$\left.\frac{\partial^2\hat{N}_0}{\partial N_k^2}\right|_{\bar{N}_k} = 0, \tag{12}$$

which can be understood by noting that the extraction of the mean intensity signal given by Eq. (3) is essentially a linear process. Consequently, all of the higher order derivatives are also equal to zero. Substitution of Eq. (12) into Eq. (11) leads to the following result:

$$b\left(\hat{N}_0\right) = 0. \tag{13}$$

Namely, the mean intensity estimator is an unbiased estimator. Note that this result is the same as that in Talbot–Lau interferometer.[28]

2.4. Bias of the first-order visibility estimator

For interferometers consisting of two $\pi/2$-shifting gratings, the first-order harmonic always contributes dominantly to the fringe intensity.[8,11] Based upon the closed-form solution of $\hat{N}_1$ given by Eq. (4), one can calculate the second-order derivative of $\hat{N}_1$ with respect to N_k as

$$\left.\frac{\partial^2\hat{N}_1}{\partial N_k^2}\right|_{\bar{N}_k} = \frac{4}{M^2\bar{N}_1}\sin^2\left(\bar{\phi}+\frac{2\pi k}{M}\right). \tag{14}$$

On the other hand, the measured photon number always follows the Poisson distribution for those photon-counting x-ray imaging systems. As a consequence, the variance of the measured phase-stepping data equals its mean value, namely,

$$\begin{aligned}\sigma_{\bar{N}_k}^2 = \bar{N}_k =\ & \bar{N}_0 + \bar{N}_1\cos\left(\bar{\phi}+\frac{2\pi k}{M}\right) \\ & + \bar{N}_2\cos\left(2\bar{\phi}+\frac{4\pi k}{M}\right).\end{aligned} \tag{15}$$

Substitution of Eqs. (14) and (15) into Eq. (11) leads to the bias of the first-order amplitude estimator

$$b\left(\hat{N}_1\right) \cong \frac{1}{2}\sum_{k=1}^{M}\left.\frac{\partial^2\hat{N}_1}{\partial N_k^2}\right|_{\bar{N}_k}\sigma_{\bar{N}_k}^2 = \frac{1}{M\bar{V}_1}\left(1-\frac{\bar{V}_2}{2}\right), \tag{16}$$

where $\bar{V}_1 = \bar{N}_1/\bar{N}_0$ and $\bar{V}_2 = \bar{N}_2/\bar{N}_0$ are the mean values of the first-order and second-order visibilities, respectively. Equation (16) suggests that the first-order amplitude estimator is positively biased, and the bias is inversely proportional to the total number of phase steps, and dependent on the mean visibilities $\bar{V}_1$ and $\bar{V}_2$. Compared to Talbot–Lau interferometer,[28] the bias of $\hat{N}_1$ is reduced to some extent, depending on the value of $\bar{V}_2$. Moreover, since it is the visibility signal that is used to define the dark-field signal, it becomes necessary to directly study the potential bias of the visibility estimator. By using the closed-form solution of $\hat{V}_1$ given by Eq. (6), one can compute the second-order derivative of $\hat{V}_1$ with respect to N_k as

$$\left.\frac{\partial^2 \hat{V}_1}{\partial N_k^2}\right|_{\bar{N}_k} = \frac{2}{(M\bar{N}_0)^2}\left[\frac{2}{\bar{V}_1} + \bar{V}_1 - 2\cos\left(\bar{\phi} + \frac{2\pi k}{M}\right) - \frac{2}{\bar{V}_1}\cos^2\left(\bar{\phi} + \frac{2\pi k}{M}\right)\right]. \tag{17}$$

On substitution of Eqs. (15) and (17) into Eq. (11), with a few straightforward calculations, the bias of the first-order visibility estimator $\hat{V}_1$ is found to be

$$b\left(\hat{V}_1\right) \cong \frac{1}{M\bar{N}_0\bar{V}_1}\left(1 - \frac{\bar{V}_2}{2}\right), \tag{18}$$

which reveals that the first-order visibility estimator is also positively biased, with the bias level inversely proportional to the product of the total number of phase steps and the mean number of photons counted per phase step. Moreover, the bias level is always dependent on the mean visibilities $\bar{V}_1$ and $\bar{V}_2$. In comparison with Talbot–Lau interferometer,[28] the bias of the first-order visibility estimator is reduced by a factor of $\bar{V}_2/2$.

2.5. Bias of the second-order visibility estimator

For interferometers that consist of dual π-shifting gratings, the second-order harmonic dominates the contribution to the fringe intensity.[8,11] Using the closed-form solution of $\hat{N}_2$ given by Eq. (5), one can readily obtain the second-order derivative of $\hat{N}_2$ with respect to N_k as

$$\left.\frac{\partial^2 \hat{N}_2}{\partial N_k^2}\right|_{\bar{N}_k} = \frac{4}{M^2\bar{N}_2}\sin^2\left(2\bar{\phi} + \frac{4\pi k}{M}\right). \tag{19}$$

On substitution of Eqs. (15) and (19) into Eq. (11), one obtains the bias of the second-order amplitude estimator

$$b\left(\hat{N}_2\right) \cong \frac{1}{M\bar{V}_2}\left[1 - \frac{\bar{V}_1}{2}\cos\left(5\bar{\phi}\right)\delta_{5,M} - \frac{\bar{V}_2}{2}\cos\left(6\bar{\phi}\right)\delta_{6,M}\right], \tag{20}$$

where $\delta_{i,j}$ is the Kronecker delta function. Equation (20) demonstrates that the positive bias can be dependent on the mean phase $\bar{\phi}$ in the case of $M = 5$ or $M = 6$. With $M > 6$, the bias is only determined by the total number of phase steps and the mean second-order visibility. Furthermore, we consider the potential bias of the second-order visibility estimator on the basis of Eq. (20). After a few straightforward calculations, the bias of the second-order visibility estimator is shown to be

$$b\left(\hat{V}_2\right) \cong \frac{1}{M\bar{N}_0\bar{V}_2}\left[1 - \frac{\bar{V}_1}{2}\cos\left(5\bar{\phi}\right)\delta_{5,M} - \frac{\bar{V}_2}{2}\cos\left(6\bar{\phi}\right)\delta_{6,M}\right], \tag{21}$$

which shows that the second-order visibility estimator is also positively biased, with the bias level dependent on the mean phase through $\cos\left(5\bar{\phi}\right)$ with $M = 5$, and through $\cos\left(6\bar{\phi}\right)$ in the case of $M = 6$. With $M > 6$, the bias level is inversely proportional to the total number of photons counted $M\bar{N}_0$ and the mean visibility $\bar{V}_2$, and independent of the mean visibility $\bar{V}_1$. Note that in the case of $M > 6$, the biases given by Eqs. (20) and (21) are the same as those in Talbot–Lau interferometer.[28]

3. Validation results

In order to validate theoretical formulas of estimation biases, numerical experiments are performed by using parameters that resemble those used in recent experimental measurements.[16] Phase-stepping data was generated following the theoretical model given by Eq. (1). Especially, the simulated mean visibilities $\bar{V}_1$ and $\bar{V}_2$ had realistic values of 0.15 and 0.3, respectively, according to experimental measurements.[16] Besides, the mean number of photons counted per phase step $\bar{N}_0$ ranged from 200 to 2000, and the total number of phase steps M ranged from 5 to 11. Finally, photon shot noise, the main factor affecting the quality of dark-field images, was considered in the generated phase-stepping data to make the simulations more realistic.

For given values of $\bar{N}_0$ and M, the phase-stepping measurements were repeated 500 times for statistical significance. According to the data processing procedure,[28,29] the 500 sets of phase-stepping data were averaged at each phase step to obtain $\bar{N}_k(x,y)$, to which the least-squares fitting algorithm was applied to estimate $\bar{N}_0$, $\bar{N}_1$, $\bar{N}_2$, $\bar{V}_1$ and $\bar{V}_2$. On the other hand, the least-squares fitting algorithm was applied to each set of phase-stepping data to estimate the multi-contrast signals $\{\hat{N}_0, \hat{N}_1, \hat{N}_2, \hat{V}_1, \hat{V}_2\}$. Then ensemble averaging was performed for each estimator to obtain $\langle\hat{N}_0\rangle$, $\langle\hat{N}_1\rangle$, $\langle\hat{N}_2\rangle$, $\langle\hat{V}_1\rangle$ and $\langle\hat{V}_2\rangle$. Finally, the estimation bias was calculated by the difference, and compared to the theoretically predicted values.

3.1. Validation of $b\left(\hat{N}_0\right)$

According to the data processing procedure and the signal extraction formula given by Eq. (3), $\bar{N}_0$ and $\langle\hat{N}_0\rangle$ are respec-

tively calculated by

$$\bar{N}_0 = \frac{1}{M}\sum_{k=1}^{M}\bar{N}_k = \frac{1}{M}\sum_{k=1}^{M}\frac{1}{500}\sum_{j=1}^{500}N_k^{(j)} = \frac{1}{500}\frac{1}{M}\sum_{k=1}^{M}\sum_{j=1}^{500}N_k^{(j)}, \tag{22}$$

$$\langle\hat{N}_0\rangle = \frac{1}{500}\sum_{j=1}^{500}\hat{N}_0^{(j)} = \frac{1}{500}\sum_{j=1}^{500}\frac{1}{M}\sum_{k=1}^{M}N_k^{(j)} = \frac{1}{500}\frac{1}{M}\sum_{j=1}^{500}\sum_{k=1}^{M}N_k^{(j)}, \tag{23}$$

where $N_k^{(j)}$ denotes the j^{th} repeated intensity measurement at the k^{th} phase step, and $\hat{N}_0^{(j)}$ denotes the estimated $\hat{N}_0$ from the j^{th} phase-stepping data by using Eq. (3). Then the bias of $\hat{N}_0$ is calculated as

$$b\left(\hat{N}_0\right) = \langle\hat{N}_0\rangle - \bar{N}_0 = 0. \tag{24}$$

Namely, $\hat{N}_0$ is an unbiased estimator. Actually, this is a direct result of the fact that the extraction of the mean intensity signal given by Eq. (3) is a linear process.

3.2. Validation of $b\left(\hat{N}_1\right)$

Figure 1(a) shows the logarithm of the bias $b\left(\hat{N}_1\right)$ against the logarithm of the number of phase steps for different mean numbers of photons counted per phase step, along with theoretical predictions by Eq. (16). In all cases, the estimation bias $b\left(\hat{N}_1\right)$ obtained through numerical simulations is in accordance with theoretical values given by Eq. (16). As expected, the positive bias $b\left(\hat{N}_1\right)$ is inversely proportional to the number of phase steps, and independent of the mean number of photons counted per phase step. This behavior is further confirmed by the results shown in Fig. 1(b), where the bias of $\hat{N}_1$ is plotted as a function of the mean number of photons counted per phase step for three different numbers of phase steps. The error bars in Fig. 1 represent the standard deviation of ensemble averaging. Generally, the numerical results are consistent with theoretical predictions with an increase in the mean photon number $\bar{N}_0$. With a smaller mean photon number, minor deviations are observed between numerical results and theoretical mean values. These deviations can be mainly induced by noise from photon statistics, and the truncation of the Taylor series expansion after the second order. A comparison between Figs. 1(b) and 3(b) shows that the photon noise influences the estimation bias greater in the case of a lower mean visibility. With a further increasing repetition of phase-stepping measurements, the remaining deviation will continue to decrease. Despite slight deviations, theoretically predicted values are always comparable to numerical results, falling within one standard deviation for all mean photon numbers. The good agreement confirms the validity of the theoretical formula of Eq. (16).

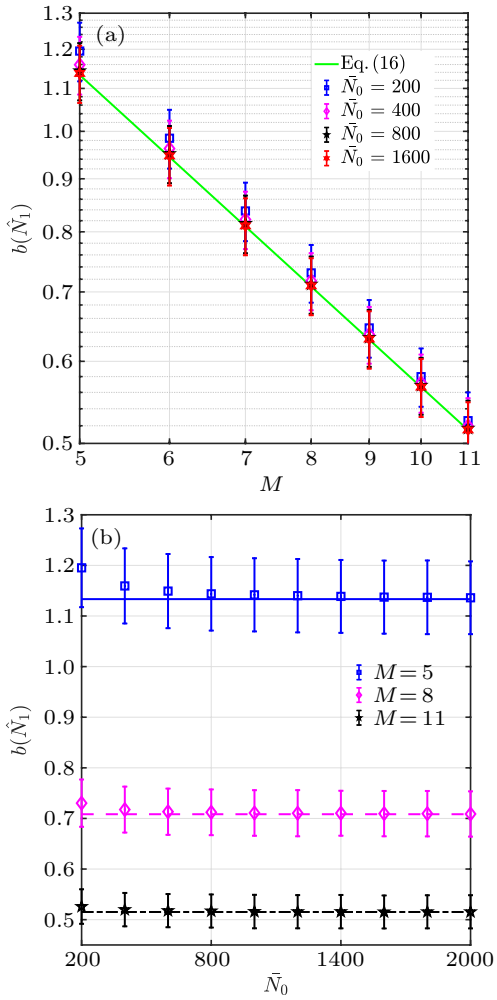


Fig. 1. (a) Log–log plot of $b\left(\hat{N}_1\right)$ against the total number of phase steps for different mean photon numbers per phase step. (b) Plot of $b\left(\hat{N}_1\right)$ as a function of the mean number of photons counted per phase step for different numbers of phase steps.

3.3. Validation of $b\left(\hat{V}_1\right)$

Figure 2(a) presents the logarithm of the bias $b\left(\hat{V}_1\right)$ against the logarithm of the number of phase steps for different mean numbers of photons counted per phase step, together with theoretical predictions from Eq. (18). It is seen that the numerical results (represented by points with error bars) agree quite well with theoretical predictions (represented by solid lines) in all cases. As expected, the bias $b\left(\hat{V}_1\right)$ decreases linearly with the inverse of the number of phase steps. Figure 2(a) also suggests that different from $b\left(\hat{N}_1\right)$, the bias $b\left(\hat{V}_1\right)$ is dependent on the mean number of photons counted per phase step. This behavior is further investigated in Fig. 2(b), where the logarithm of the bias $b\left(\hat{V}_1\right)$ is plotted against the logarithm of the mean number of photons counted per phase step for different values of M, along with theoretical predictions from Eq. (18). As shown, there is an excellent agreement between numerical results and theoretical predictions. Indeed, the bias $b\left(\hat{V}_1\right)$ decreases linearly with the inverse of the mean photon number $\bar{N}_0$. The error bars in Fig. 2 are from the standard

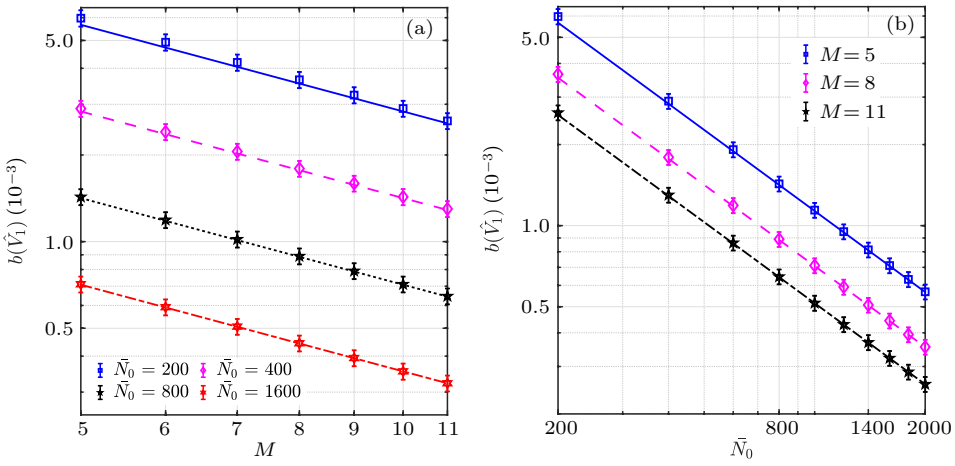


Fig. 2. (a) Log–log plot of $b\left(\hat{V}_1\right)$ against the number of phase steps M for different mean photon number $\bar{N}_0$ per phase step. (b) Log–log plot of $b\left(\hat{V}_1\right)$ against the mean number of photons counted per phase step $\bar{N}_0$ for different values of M.

deviation of ensemble averaging. The results shown in Fig. 2 means that the overall number of photons counted, $M \times \bar{N}_0$, is the determining factor of the bias $b\left(\hat{V}_1\right)$. All these results confirm the validity of Eq. (18).

3.4. Validation of $b\left(\hat{N}_2\right)$

In Fig. 3(a), the logarithm of the bias $b\left(\hat{N}_2\right)$ is drawn against the logarithm of the number of phase steps for different mean numbers of photons counted per phase step. As can be seen, the bias $b\left(\hat{N}_2\right)$ obtained through numerical simulations

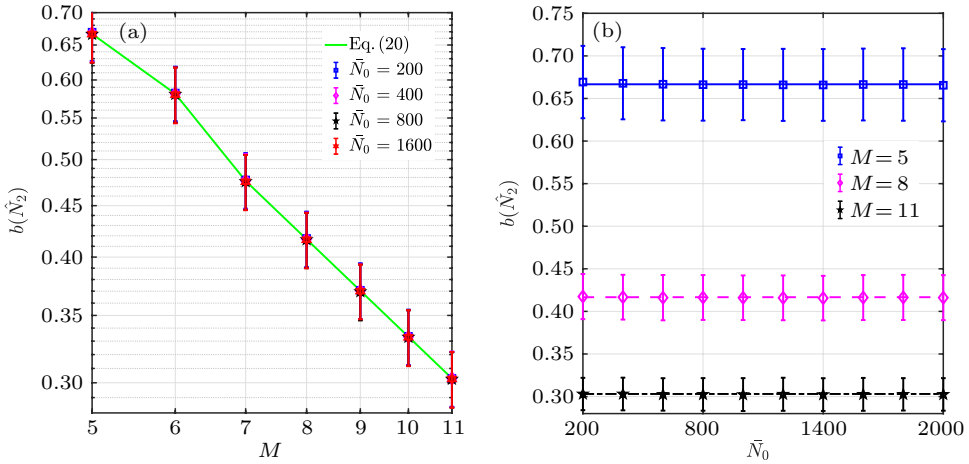


Fig. 3. (a) Log–log plot of $b\left(\hat{N}_2\right)$ against the total number of phase steps for different mean numbers of photons counted per phase step. (b) Plot of $b\left(\hat{N}_2\right)$ as a function of the mean number of photons counted per phase step for different numbers of phase steps.

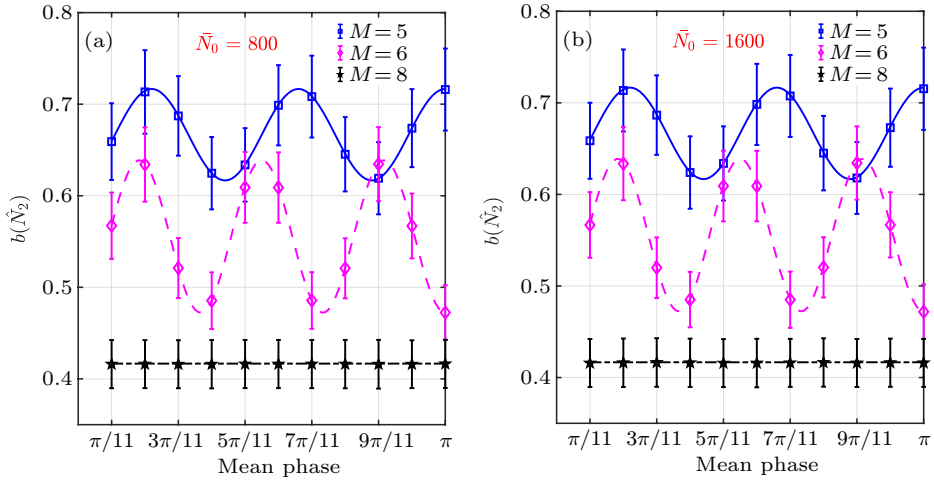


Fig. 4. Plot of $b\left(\hat{N}_2\right)$ as a function of the mean phase for given number of phase steps. The mean number of photons counted per phase step is (a) 800 and (b) 1600.

is in good agreement with theoretical predictions by Eq. (20) in all cases. As expected, the positive bias $b\left(\hat{N}_2\right)$ is linearly dependent on the reciprocal number of the phase step number M, and independent of the mean number of photons counted per phase step. This behavior is further confirmed by the results presented in Fig. 3(b), where the bias of $\hat{N}_2$ is plotted across different mean numbers of photons counted per phase step. As shown in Fig. 3(b), for a given number of phase steps, the bias $b\left(\hat{N}_2\right)$ remains almost constant with an increase in the mean photon number $\bar{N}_0$. The error bars in Fig. 3 represent the standard deviation of ensemble averaging. These results validate the theoretical formula of Eq. (20).

To further validate Eq. (20), Fig. 4 shows the bias $b\left(\hat{N}_2\right)$ as a function of the mean phase for given values of M and mean photon number $\bar{N}_0$ per phase step. As can be seen, the bias of $\hat{N}_2$ oscillates as a function of the mean phase with $M = 5$ or $M = 6$, and shows no dependence on the mean phase with $M = 8$. All these results are consistent with theoretical predictions from Eq. (20).

3.5. Validation of $b\left(\hat{V}_2\right)$

Figure 5(a) shows the logarithm of the bias $b\left(\hat{V}_2\right)$ with respect to the logarithm of the number of phase steps for different mean numbers of photons counted per phase step, together with theoretical predictions from Eq. (21). A good agreement is found between numerical results (represented by points with error bars) and theoretical predictions (represented by solid lines) in all considered cases. A linear decrease of the positive bias $b\left(\hat{V}_2\right)$ can be observed with the inverse of the number of phase steps. Moreover, different from $b\left(\hat{N}_2\right)$, the bias $b\left(\hat{V}_2\right)$ also shows dependence on the mean photon number $\bar{N}_0$. This behavior is further investigated, and the results are presented in Fig. 5(b). As demonstrated, good agreement can be found between numerical results and theoretical predictions from Eq. (21). The logarithm of the bias $b\left(\hat{V}_1\right)$ decreases linearly with the logarithm of the mean number of photons counted per phase step for a given number of phase steps. This is, the bias $b\left(\hat{V}_2\right)$ is inversely proportional to the mean photon number $\bar{N}_0$. The results shown in Fig. 5 prove that it is the overall number of photons counted, $M \times \bar{N}_0$, that determines the bias of the estimator $\hat{V}_2$. The error bars in Fig. 5 are from the standard deviation of ensemble averaging. All these results validate the theoretical formula of Eq. (21).

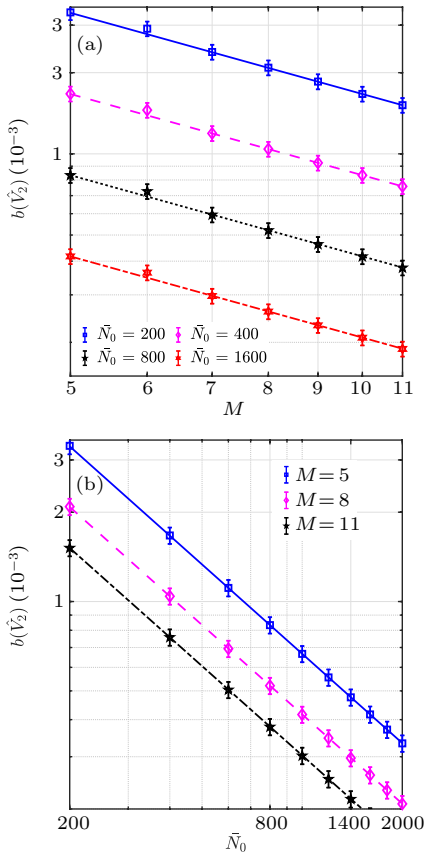


Fig. 5. (a) Log–log plot of $b\left(\hat{V}_2\right)$ against the number of phase steps M for different mean photon number per phase step $\bar{N}_0$. (b) Log–log plot of $b\left(\hat{V}_2\right)$ against the mean photon number $\bar{N}_0$ per phase step for different values of M.

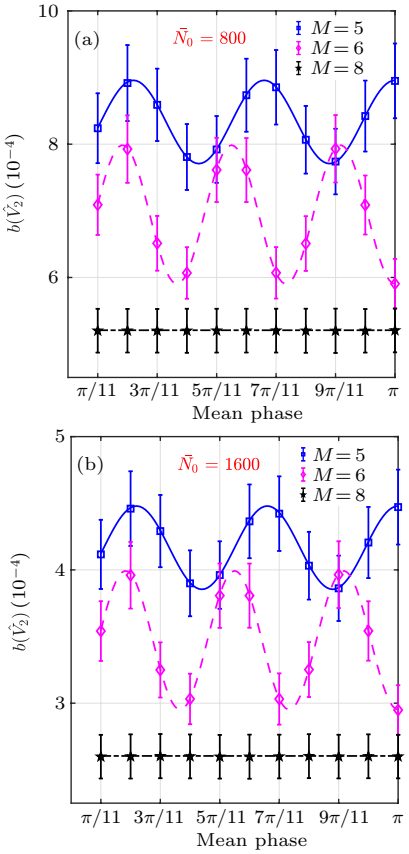


Fig. 6. Plot of $b\left(\hat{V}_2\right)$ as a function of the mean phase for given number of phase steps, with the mean photon number per phase step $\bar{N}_0$ being (a) 800 and (b) 1600.

For further validation, the bias of $\hat{V}_2$ is drawn as a function of the mean phase and the number of phase steps in Fig. 6. With the number of phase steps M being 5 or 6, a sinusoidal oscillation of $b\left(\hat{V}_2\right)$ as a function of the mean phase is observed. In the case of $M = 8$, the bias $b\left(\hat{V}_2\right)$ remains almost

constant with an increase of the mean phase. All these numerical results demonstrate a good agreement with theoretical predictions from Eq. (21).

4. Discussion and conclusion

This work investigated the potential biases of x-ray multi-contrast signals extracted using the least-squares fitting algorithm, as given by Eqs. (3)–(5). Analytical formulas of estimation biases were derived by using a second-order Taylor series expansion, and validated by a series of numerical simulations. It was shown that there was no bias for the absorption related signal $\hat{N}_0$. For the dark-field related signals $\hat{N}_1$ and $\hat{N}_2$, the bias was always positive, with the bias level proportional to the inverse of the total number of phase steps and dependent on the mean visibilities $\bar{V}_1$ and $\bar{V}_2$. To further understand the practical implications of the biases, it is beneficial to investigate the relative error introduced by the bias, namely,

$$\frac{b\left(\hat{N}_1\right)}{\bar{N}_1} = \frac{1}{M\bar{N}_0}\left[\frac{1}{\bar{V}_1^2}\left(1-\frac{\bar{V}_2}{2}\right)\right], \tag{25}$$

$$\frac{b\left(\hat{N}_2\right)}{\bar{N}_2} = \frac{1}{M\bar{N}_0}\left\{\frac{1}{\bar{V}_2^2}\left[1-\frac{\bar{V}_1}{2}\cos\left(5\bar{\phi}\right)\delta_{5,M} - \frac{\bar{V}_2}{2}\cos\left(6\bar{\phi}\right)\delta_{6,M}\right]\right\}. \tag{26}$$

From Eq. (16) and (20), it could be misleading to conclude that more phase steps would reduce the biases. Actually, for a given value of $M\bar{N}_0$ (proportional to the total exposure level), the relative error was dominantly determined by the mean visibilities $\bar{V}_1$ and $\bar{V}_2$. This fact emphasizes the significance of improving the visibility of dual phase grating interferometers. Under the condition of a fixed total exposure level, an increase in the total number of phase steps would not influence the relative bias.

For the visibility signals $\hat{V}_1$ and $\hat{V}_2$, the biases were inversely proportional to the product of the total number of phase steps M and the mean number of photons counted per phase step $\bar{N}_0$. Additionally, the biases decreased with an increase in the mean visibilities. Therefore, for grating interferometers with acquisition parameters of $M \geq 5$, $\bar{N}_0 \geq 200$, and mean visibilities $\bar{V}_i \geq 0.1$ $(i = 1, 2)$, the biases of visibility signals were less than 0.01 and thus can be considered negligible. By contrast, if the total exposure level satisfied the condition of $M\bar{N}_0\bar{V}_i \ll 100$, the biases would be much greater than 0.01 and thus must be taken into consideration for image interpretation.

Since both the signal standard deviation and signal bias contribute to the overall variability of the visibility signal, it would be interesting to compare the relative amplitude of these two contributions. The signal standard deviation can be derived by using Eqs. (6) and (7) and error propagation formula.[30] Then one can calculate the ratio between the bias and the standard deviation of the visibility signal. These investigations will be left for future work. Finally, the main limitation of this study is the lack of experimental data, with further validation currently being planned.

In summary, we have investigated the potential biases of multi-contrast signals in x-ray dark-field imaging using dual phase grating interferometer. Analytical expressions of estimation biases were theoretically derived by using a second-order Taylor series expansion to quantify the level of biases and the dependence of signal biases on data acquisition parameters. Theoretical formulas were validated by extensive numerical simulations. It was demonstrated that while the estimated mean intensity signal was always unbiased, the estimated amplitude and visibility signals were positively biased. And the biases were inversely proportional to the total number of phase steps and the mean number of photons counted per phase step. Besides, the biases decreased with increased visibilities of dual phase grating interferometers. Finally, due to the difference in intensity model, the estimation biases of amplitude and visibility signals were different from those of Talbot–Lau interferometers. We expect that these results can be used as guidelines for data acquisition optimizations and dark-field image interpretation.

Acknowledgements

Project supported by the National Natural Science Foundation of China (Grant Nos. U1532113, 11475170, and 11905041), Anhui Provincial Natural Science Foundation (Grant No. 2208085MA18), and Fundamental Research Funds for the Central Universities (Grant No. JZ2022HGTB0244).

References

[1] Miao M, Panna A, Gomella A, Bennett E, Znati S, Chen L and Wen H 2016 *Nat. Phys.* **12** 830
[2] Kagias M, Wang Z, Jefimovs K and Stampanoni M 2017 *Appl. Phys. Lett.* **110** 014105
[3] Yan A, Wu X and Liu H 2018 *Opt. Express* **26** 23142
[4] Yan A, Wu X and Liu H 2019 *Opt. Express* **27** 22727
[5] Yan A, Wu X and Liu H 2019 *Opt. Express* **27** 35437
[6] Ge Y, Chen J, Zhu P, Yang J, Deng S, Shi W, Zhang K, Guo J, Zhang H, Zheng H and Liang D 2020 *Opt. Express* **28** 9786
[7] Pandeshwar A, Kagias M, Wang Z and Stampanoni M 2020 *Opt. Express* **28** 19187
[8] Yan A, Wu X and Liu H 2020 *J. X-ray Sci. Technol.* **28** 1055
[9] Ge Y, Chen J, Yang J, Zhu P, Zhang H, Zheng H and Liang D 2021 *Opt. Lett.* **46** 2791
[10] Wang Z, Zhou R, Zhao L, Ren K, Xu W, Liu B and Chen H 2021 *Chin. Phys. B* **30** 028702
[11] Organista C, Kagias M, Tang R, Shi Z, Jefimovs K, Boone M and Stampanoni M 2023 *Opt. Continuum* **2** 232
[12] Tang R, Organista C, Goethals W, Stolp W, Stampanoni M, Aelterman J and Boone M 2023 *Opt. Express* **31** 1677
[13] Tang R, Organista C, Romano L, Van Hoorebeke L, Stampanoni M, Aelterman J and Boone M 2023 *Opt. Express* **31** 40450
[14] Cai X, Tan Y, Zhang X, Yang J, Xu J, Zheng H, Liang D and Ge Y 2023 *Opt. Express* **31** 44273
[15] Tang R, Goethals W, Organista C, Van Hoorebeke L, Stampanoni M, Aelterman J and Boone M 2024 *Opt. Express* **32** 14607

[16] Organista C, Tang R, Shi Z, Jefimovs K, Josell D, Romano L, Spindler S, Kibleur P, Blykers B, Stampanoni M and Boone M 2024 *Sci. Rep.* **14** 384
[17] Weitkamp T, Diaz A, David C, Pfeiffer F, Stampanoni M, Cloetens P and Ziegler E 2005 *Opt. Express* **13** 6296
[18] Pfeiffer F, Weitkamp T, Bunk O and David C 2006 *Nat. Phys.* **2** 258
[19] Pfeiffer F, Bech M, Bunk O, Kraft P, Eikenberry E F, Brönnimann C H, Grünzweig C and David C 2008 *Nat. Mater.* **7** 134
[20] Yang J, Guo J C, Lei Y H, Yi M H and Chen L 2017 *Chin. Phys. B* **26** 028701
[21] Wei C X, Wu Z, Fazi W, Wei W B, Bao Y, Luo R H, Wang L, Liu G and Tian Y C 2017 *Chin. Phys. B* **26** 108701
[22] Rong F, Gao Y, Guo C J, Xu W and Xu W 2019 *Chin. Phys. B* **28** 108702
[23] Faiz W, Li J, Gao K, Wu Z, Lei Y H, Huang J H and Zhu P P 2020 *Chin. Phys. B* **29** 014301
[24] Yang J, Huang J H, Lei Y H, Zheng J B, Shan Y Z, Guo D Y and Guo J C 2022 *Chin. Phys. B* **31** 058701
[25] Yashiro W, Terui Y, Kawabata K and Momose A 2010 *Opt. Express* **18** 16890
[26] Strobl M 2014 *Sci. Rep.* **4** 7243
[27] Weber T, Bartl P, Bayer F, Durst J, Haas W, Michel T, Ritter A and Anton G 2011 *Med. Phys.* **38** 4133
[28] Ji X, Ge Y S, Zhang R, Li K and Chen G H 2017 *Med. Phys.* **44** 2453
[29] Xia J, Xu W, Zhou R, Shi X, Ren K, Chen H and Wang Z 2020 *Chin. Phys. B* **29** 068703
[30] Wang Z, Xu W, Wang T, Ren K, Zhao L, Liu B and Chen H 2021 *Nucl. Instrum. Meth. A* **995** 165113